Practically achievable process performance limits for pressure-vacuum swing adsorption based post-combustion CO_2 capture

Kasturi Nagesh Pai, Vinay Prasad, and Arvind Rajendran[a]

Department of Chemical and Materials Engineering, University of Alberta, 12th Floor, Donadeo Innovation Centre for Engineering (ICE), 9211 - 116 Street, Edmonton, Alberta, CANADA, T6G 1H9

E-mail: *arvind.rajendran@ualberta.ca

[a]Correspondence concerning this article should be addressed to A. Rajendran at this current address: Department of Chemical and Materials Engineering, University of Alberta, 12th Floor, Donadeo Innovation Centre for Engineering (ICE), 9211 - 116 Street, Edmonton, Alberta, CANADA, T6G 1H9

Abstract

Practically achievable limits for pressure-vacuum swing adsorption (PVSA)-based post-combustion carbon capture are evaluated. The adsorption isotherms of CO_2 and N_2 are described by competitive Langmuir isotherms. Two low-energy process cycles are considered and a machine learning surrogate-model is trained with inputs from an experimentally-validated detailed PVSA model. Several case studies are considered to evaluate two critical performance indicators, namely, minimum energy and maximum productivity. For each case study, the genetic algorithm optimizer that is coupled to the machine learning surrogate model, searches tens of thousands of combinations of isotherms and process operating conditions. The framework pairs the optimum material properties with the optimum operating conditions, hence providing the limits of achievable performance. The results indicate that very low pressures (< 0.2 bar) may be required to achieve process constraints for low feeds with low feed compositions (< 0.15 mol fraction), indicating that PVSA may not be favourable. At higher CO_2 feed compositions, PVSA can be attractive and can be operated at practically achievable vacuum levels. Further, the gap between the energy consumption of available adsorbents and the achievable limits with a hypothetical -best adsorbent varies between 20% to 2.5% as the CO_2 feed composition changes between 0.05 to 0.4. This indicates a limited potential for development of new adsorbents of PVSA-based CO_2 capture. Future work for PVSA should focus on flue gas streams with high CO_2 compositions

Introduction

Carbon capture and storage (CCS) is a critical component of the suite of technologies needed to fulfill the goals of the Paris agreement[1]. Carbon capture, i.e., concentrating CO_2 from flue gas or other intermediate streams, is the most expensive step in the CCS chain. Reducing the cost of capture is critical to the large-scale deployment of CCS[2]. Post-combustion CO_2 capture refers to the concentration of CO_2 from flue gas that contains N_2, CO_2 and other impurities. Absorption using liquid solvents, typically amines and their derivatives, is currently the preferred industrial technology for large-scale CO_2 capture. High regeneration costs, degradation of the solvent, and equipment corrosion are significant bottlenecks that have motivated researchers to look for alternatives[2]. Carbon capture using solid adsorbents is one such promising alternative. These adsorbents can be deployed in both pressure-vacuum swing adsorption (PVSA) or temperature swing adsorption (TSA) processes[2,3]. The advent of novel adsorbents, such as metal-organic frameworks (MOFs), and covalent organic frameworks (COFs), has intensified the search for suitable capture materials[2,4].

Traditionally, the selection of adsorbents has heavily relied on simplified process metrics that are calculated from simple equilibrium measurements/ calculations. However, in recent years, there seems to be a consensus that these metrics are not reliable and that detailed process simulations and optimization essential to reliably evaluate the true separation potential of adsorbents[5–10]. Exploring this adsorbent-process relationship can be classified into two approaches: screening and process inversion. In screening, the critical question is, *"If we know the characteristics of an adsorbent, what is the best process outcome that can be achieved?"*. Both simple and detailed process models have been used for screening, and a variety of studies have been published[6,7,11–13]. In process inversion, the central question is: *"What should be the characteristic of the adsorbent that produces the best process outcome?"*. A few studies have explored this *"inverse"* problem. Maring and Webley used a simplified batch-adsorber model to vary adsorbent-specific properties such as Henry's constant and heat of adsorption to explore the features of an adsorbent that minimizes energy[14]. Ra-

jagopalan and Rajendran used detailed models to explore how the competitive nature of CO_2 and N_2 impacts the separation and identified regions where low energy consumption can be achieved[15]. Danaci extended the Maring-Webley model and explored adsorbent features that would minimize the cost of capture[16]. Khurana and Farooq used detailed process models and examined the characteristics of the CO_2 and N_2 isotherms that enhance process performance[12] and cost[17] for the case of post-combustion CO_2 capture from coal plants.

The above-mentioned studies have allowed the scientific community to make progress in understanding the relationship between adsorbent characteristics and process performance. While this pursuit is far from over,[10] the question *"What are the best performance indicators, namely energy consumption and productivity, that are practically achievable by using adsorption processes?"* remains open. While the (technology-agnostic) thermodynamic minimum energy consumption, based on the free-energy of mixing, is undoubtedly helpful, it is well known that practical separation processes consume significantly higher energy compared to these values. It is, in fact, the practically achievable minimum energy and maximum productivity values that will permit objective technology evaluation. These limits also indicate the *"innovation potential"* that is possible, thereby providing useful information to both materials chemists and process engineers. It is worth noting that such limits, for the case of adsorption, are currently not known. In this work, we restrict ourselves to the case of pressure-vacuum swing adsorption (PVSA) applied to post-combustion CO_2 capture, a class of adsorption process that has been extensively studied. Accordingly, the critical question that we seek to answer in this work is *"If we can design the ideal adsorbent(s), what are the practically achievable limits of minimum energy and maximum productivity for PVSA?"*.

It is well known that adsorption process simulations are time-consuming, and hence deploying them for large-scale optimization and screening remains a challenge[10,18]. In this work, we exploit recent innovations in machine learning to accelerate adsorption process simulations[19]. Specifically, we employ the machine-assisted process learning and evaluation (MAPLE) framework, a data-driven modelling framework trained using a detailed process

model suitable for accepting both process operating conditions and adsorbent properties as inputs[20]. Several case studies are presented to explore the operation, performance, and material limits.

Methodology

Separation System and Performance Metrics: CO_2 capture is modelled as the separation and concentration of CO_2 from a binary gas mixture of CO_2 and N_2. While most flue gas contains impurities including, water, we assume that they are removed upstream of the capture unit. This seems reasonable since most adsorbents, barring a few exceptions, adsorb water strongly, and their performance is likely to deteriorate in the presence of water. The CO_2 purity, Pu_{CO_2}= (moles of CO_2 in the product)/(moles of CO_2 + N_2 in the product) $\times$ 100 [%] and CO_2 recovery, Re_{CO_2}=(moles of CO_2 in the product)/(moles of CO_2 in the feed) $\times$ 100 [%] are important metrics to evaluate CO_2 capture performance. The US-Department of Energy (US-DOE) targets require $Pu_{CO_2} \geq 95\%$ and $Re_{CO_2} \geq 90\%$. The key performance metrics that are used to evaluate the process include energy consumption, En =(energy consumption / tonne CO_2 captured) the process productivity, Pr =(moles of CO_2 captured/ unit volume of adsorbent/second). It is worth noting that a proper scale-up and techno-economic analysis is required to evaluate the potential of any capture technology[17,21]. However, since the cost of many novel adsorbents is not known, full-scale costing may not be feasible without making assumptions. Under such circumstances, energy and productivity estimates are valuable in making critical decisions about technology selection and evaluation.

PVSA Process Modelling: The accurate modelling of an adsorbent-based separation process requires a detailed description of mass and heat transfer and fluid dynamics. Since adsorptive processes are inherently cyclic, the equations describing each step are iteratively solved until a cyclic steady state. In this study, we keep the column dimensions and the sizes

of fluid movers fixed to match the scale of a PVSA-based CO_2 capture pilot plant described Krishnamurthy et al.[22]. The model is based on the following key assumptions: 1. The ideal gas law is obeyed; 2. An axially dispersed plug flow model describes the flow in the column; 3. The solid and fluid phases are in thermal equilibrium, and that the column is assumed to be adiabatic; 4. The adsorbent is assumed to be particles of 2 mm in diameter. Mass transfer is described by a linear-driving force (LDF) model, assuming that the molecular diffusion in macropores controls the mass transfer; 5. Darcy's law is used to describe the pressure drop in the column (It has been shown that for the current process scale under investigation and the operating conditions studied, this assumption is satisfactory). The column mass and energy balances result in a system of partial differential equations (PDEs). The PDEs are reduced to ordinary differential equations (ODEs) system using a finite-volume scheme. They are solved using *ode23s*, an inbuilt solver in MATLAB. Appropriate boundary conditions are applied for the specific step. Model equations and boundary conditions are provided in the supporting information. Properties associated with the column are provided in Table 1. The entire simulation strategy is detailed in a previous work[23] and validated experimentally both at lab-scale[24] and pilot-scales[22].

In this study, we use a constant-selectivity single-site Langmuir (SSL) isotherm to describe the competitive adsorption equilibrium:

$$q_i^* = \frac{q_{\text{sat}} b_i C_i}{1 + b_{\text{CO}_2} C_{\text{CO}_2} + b_{\text{N}_2} C_{\text{N}_2}} = \frac{H_i C_i}{1 + b_{\text{CO}_2} C_{\text{CO}_2} + b_{\text{N}_2} C_{\text{N}_2}}, , \ i = \text{CO}_2, \text{N}_2 \tag{1}$$

where q_{sat} is the saturation capacity, b_i is the equilibrium constant for component i, and q_i^* is the equilibrium solid phase loading. The product of q_{sat} and b_i is the Henry constant, H_i. The temperature dependence of the equilibrium constant is described by

$$b_i = b_{0,i} e^{\frac{-\Delta U_i}{R_g T}} \tag{2}$$

where ΔU_i is the internal energy of adsorption for component i, R_g is the universal gas con-

stant and, T is the temperature. The SSL isotherm comprises of five parameters, *viz.*, q_{sat}, $b_{0,\mathrm{CO_2}}$, $b_{0,\mathrm{N_2}}$, $\Delta U_{\mathrm{CO_2}}$, and $\Delta U_{\mathrm{N_2}}$. It is worth noting that in many cases, more complicated forms of the isotherm, e.g., dual-site Langmuir, are needed to describe the equilibrium loading[25], and the use of an SSL can limit the range of isotherm behaviours that can be studied. While we acknowledge that this can be considered a limitation, it is worth pointing out that the SSL isotherm does provide a simple and elegant formulation to describe competitive behaviour for several systems of practical interest[6,26]. Further, since the isotherm uses just five parameters, it allows for the understanding and visualization of the interplay between material properties and process configurations.

Process Cycles: The PVSA processes used in this study are shown in Fig. 1. A 4-step cycle with light product pressurization (LPP) is shown in Fig. 1 a), and a 4-step cycle with feed pressurization (FP) is shown in Fig. 1 b). Both cycles consist of four steps: 1. An adsorption step, where the feed mixture consisting of y_{F} mole-fraction of CO_2, with the balance being N_2, is introduced at the feed end ($z = 0$) of the column with an interstitial feed velocity v_{F} and pressure P_{H}, for a period of t_{ADS}. The light product, which is predominantly N_2, is collected at the outlet end ($z = L$). 2. A blowdown step, where a vacuum pump removes gas from the top of the column and the column pressure is reduced to an intermediate value, P_{I}. This step aims to remove the N_2 while reducing CO_2 loss. 3. An evacuation step, where another vacuum pump further reduces the pressure to a low value, P_{L} and high purity CO_2 product is collected at the feed end ($z = 0$). 4. A pressurization step, where the pressure of the column is brought back from the P_{L} to P_{H} using either the feed stream (F) or the light-product (LP). The cycles are called 4-step with LPP and 4-step with FP depending on how the pressurization step is performed. Although the two differ in just one step, they are known to show measurably different performances[23,24]. While it is certainly possible to construct more complex cycles, we limit ourselves to these two cycles, as they have been used by several research groups as a benchmark[6,8,17,27], and they have been demonstrated in lab-scale[24] and pilot-scale experiments[22].

At a process scale, four performance indicators, $Pu_{\mathrm{CO_2}}$, $Re_{\mathrm{CO_2}}$, En, and Pr, are considered and have been defined earlier. The energy consumption for the process comes from four steps: the energy required to pressurize the gas from atmospheric pressure to the P_{H} and to overcome the pressure-drop in the column during the pressurization and adsorption steps; and the energy consumption of the vacuum pumps in the blowdown and evacuation steps. The vacuum pump efficiency, while in many process studies were fixed to $\approx 70-80\%$, is now assumed to vary with pressure according to the expression given in Table 1. The cycle-time used to calculate productivity is the sum of the duration of the four steps. Each of the pressure reduction steps has a dedicated vacuum pump that operates at a constant volumetric flow rate. This means that the duration of the blowdown (t_{BLO}) and evacuation (t_{BLO}) steps are dependent on the flow rate. Naturally, using a pump with a higher flow rate will reduce the duration but could result in a higher cost. This study considers the vacuum pump, and the column dimensions are fixed. Finally, the pressure drops in the lines can be detrimental for energy consumption for systems working under vacuum conditions. The pressure drop can result in increased energy consumption and slower evacuation, both of which will worsen the process performance. In this study, such pressure drops, external to the columns, are considered to be negligible. It is important to consider the results in light of these assumptions.

The MAPLE Framework and Process Optimization: The MAPLE framework, is a data-driven surrogate model trained to emulate an adsorbent process using supervised machine learning[20]. The main advantage of this framework lies in its ability to have both adsorbent and process-related inputs. Compared to the full models, MAPLE is orders of magnitude faster to train and deploy[20]. The operating conditions and their training ranges for the two process cycles are shown in Fig: 1 a) and b). The adsorbent and operationally related trained input space is shown in Figs. S2 and S3 of the supporting information and in Table 1. Physically meaningful constraints were applied while generating the samples. For instance, CO_2 is always the strongly adsorbed gas, i.e. $b_{\mathrm{CO_2}} \geq \mathrm{b_{N_2}} + 3.1$ [$\mathrm{m^3/mol}$]. The heat

of adsorption of CO_2 is always greater than N_2, i.e., $|\Delta U_{CO_2}| \geq |\Delta U_{N_2}| + 2$ [kJ/mol]. The ranges for the isotherm parameters were selected to cover the range of adsorbents from the carbon capture materials database[11,26]. The high pressure is always greater than the intermediate pressure ($P_H \geq P_I + 0.5$[bar]). The intermediate pressure is always greater than the low pressure ($P_I \geq P_L + 0.05$[bar]). The selectivity of the adsorbent, $\alpha = H_{CO_2}/H_{N_2}$, is in the range of $3 \leq \alpha \leq 10^7$. It is worth pointing out that the equilibrium constant b_i and ΔU are (at least weakly) correlated. However, in this study, no such constraints are imposed, implying that a hypothetical adsorbent can be defined by any random combination of the five SSL parameters. The training variables are shown along with a visual representation of the MAPLE framework in Fig: 1 c). The trained variables consist of five SSL parameters, three pressure levels (P_H, P_I, P_L), the duration of the adsorption step (t_{ADS}), feed velocity (v_F), feed concentration (y_F) and adsorbent particle density (ρ_{ADS}). Recent studies have pointed out that performance gains can be obtained by also varying particle sizes and porosities[8,27]. In this study, we settle for conservative values of these parameters that are based on commercially available materials. The dataset consisting of 50,000 samples was run in the detailed model. This data was then split into a training and testing ratio of 90:10 and the model accuracy was evaluated using the R^2_{Adj} of the test-set. A network consisting of 3 hidden layers with 30 neuron layers was chosen. A test $R^2_{Adj} \geq 0.99$ was obtained for all the performance indicators, signifying high prediction accuracy. The testing and validation results can be found in Fig S4 of the supporting information. The MAPLE model is then coupled with a genetic algorithm optimization tool non-dominated sorting genetic algorithm-II (NSGA-II) available in MATLAB for performing all the case studies described below. We call this optimization framework MAPLE-Opt.[20,28]. For each optimization, an initial population of 96× [Number of decision variables] is chosen, and MAPLE-Opt. is run for 60 generations. MAPLE-Opt. is run multiple times with varying the initial populations to avoid local minima and or stochastic variations in the final result. The optimized decision variables obtained from MAPLE-Opt. are then re-run in the detailed model until cyclic

steady state (CSS) is reached to increase the certainty of prediction. Summarizing, the final results presented in this paper are from a dynamic PVSA model.

Results and discussions

Limits for US-DOE targets: In order to compare various technologies, it is important their performance is compared only under conditions where the US-DOE targets are met. One of the continuing questions concerning PVSA processes is the low-pressure (P_{L}) required to achieve these targets. Most studies in the literature that have considered flue gas from coal, i.e., $y_{\mathrm{F}} \approx 0.12-0.15$, and have focused on vacuum swing adsorption (VSA), i.e., $P_{\mathrm{H}} = 1$, since pressurizing the flue gas, that consists mainly of N_2, was considered to be expensive. Those that have performed rigorous modelling, and experimentation, indicate that extremely low pressures, i.e., < 0.05 bar, are required to meet the US-DOE target [12,29]. Quite a few articles have rightfully questioned the feasibility of scaling-up such operations [10]. Most industrial adsorption processes operate at pressures > 0.1 bar; vacuum pump efficiencies deteriorate below this value, and the volumetric flow-rates increase requiring very large piping, valves and equipment. Some studies have suggested that this can be either overcome by pressurizing the flue gas [23] or by using multiple stages [30]. It is also generally believed that the challenge of requiring low vacuum pressures can be overcome by designing an appropriate adsorbent.

In order to explore the question "*If we were able to design a hypothetical material, what will be the maximum value of* P_{L} *that will allow us to achieve the US-DOE target?*" a series of optimization runs were performed for various values of y_{F} using the 4-step with LPP cycle. For these runs, $Pu_{\mathrm{CO_2}} \geq 95\%$, and $Re_{\mathrm{CO_2}} \geq 90\%$, were considered as constraints. Multi-objective optimization to simultaneously maximize P_{L}, and minimize P_{H} was performed for a variety of y_{F} for the 4 step with LPP process. All material and process variables used for training were considered as decision variables. The resulting Pareto curves are shown in Fig. 2. The region towards the right of the Pareto curve is infeasible. For instance, for

$y_F = 0.15$, in order to achieve US-DOE targets, a maximum P_L of ≈ 0.04 bar is required to be operated as a VSA process. Further if the lowest P_L allowed is 0.1 bar, the feed has to be pressurized at-least a value of 1.8 bar. If operation at a higher value of P_L is expected, a different cycle should be adopted or an adsorbent whose isotherms are markedly different from a Langmuir form is required. For instance, Khurana and Farooq considered a more complex dual-reflux cycle configuration that could achieve the DOE-Targets at higher P_L, albeit at the cost of significantly higher energy[31]. The figure also shows that even if the flue gas is pressurized upto 5 bar pressure, a vacuum pressure of ≈ 0.2 bar is required to barely satisfy the US-DOE target. This indicates that pressurizing the flue gas should be considered and it might be difficult to avoid vacuum operations. As expected dilute feeds require lower values of P_L at any given P_H. This study indicates that PVSA processes, merely from the requirement of avoiding deep vacuum, are unfavourable for dilute feeds.

Process limits: Four case studies were considered to identify the practically achievable performance limits and the results are plotted in Fig 3 as a function of y_F. Typical ranges of y_F (CO_2 composition in the feed stream) for flue gases from natural gas combined cycle (NGCC), coal, cement and steel plants are also highlighted for convenience[32]. For case study 1, the key question posed was "*If one can synthesize ideal hypothetical adsorbents, what are the limits of minimum energy and maximum productivity while satisfying the constraints imposed by US-DOE targets*". Hence, for this study, the optimizer considers all the operating conditions and adsorbent properties, described earlier, as decision variables with an aim to either minimize energy or maximize productivity, with Pu_{CO_2} and Re_{CO_2} as constraints. The results are shown in Fig. 3 (a) and (b). Each curve in this figure is associated with a label and parameters of the power-law expression fitted to these curves are provided in Table 2. Figure 3 (a) shows the results of the minimum energy for four different cases: the thermodynamic minimum based on the free-energy of mixing (E1)[33]; the minimum energy for a four-step with LPP with the assumption that vacuum pumps and compressors operate at 100% isentropic efficiency (E2); the minimum energy with the assumption that

vacuum pumps and compressors operate with a pressure-dependent efficiency for the cases of a four-step with LPP (E3) and four-step with FP (E4) process configurations. It is important to point out for E2, E3, and E4, each point on the Pareto curves represents a unique combination of adsorbent property and process configuration. As expected, the minimum energy reduces with the increase in y_{F}. The gap between the thermodynamic minimum and the 100% efficiency gives the limit that can be achieved with the 4-step LPP processes. It is worth noting that at low values of y_{F}, the ratio of the achievable minimum energy for the 4-step LPP process, and the thermodynamic minimum is significantly larger as compared to the ratio at higher values of y_{F}. This result demonstrates that PVSA is energetically unfavourable at low y_{F}, *even if the ideal adsorbent is deployed*. This arises from the need to deploy very low vacuum levels in order to achieve the desired purity and recovery constraints, i.e., a result that is fully consistent with the observation in Fig. 2. The gap between curves E2 and E3 indicates the impact of finite prime-mover efficiency. Over the entire range of y_{F}, the average efficiency of the pumps and compressors varies between ≈ 45 to 60%. Finally, the difference between curves E3 and E4 indicates the impact of changing the cycle configuration by just one step. This highlights why a combined search of best process configuration and adsorbent is critical. For the sake of comparison, the reboiler duty of 2.3 GJ/tonne CO_2 captured (at $Pu = 99.8\%$ and $Re = 90\%$) for a commercial absorption process, i.e., CanSOLV, is provided[34]. A reasonable thermal to electrical conversion factor of 40% is used to represent the equivalent energy in electrical units. It can be seen that for $y_{\mathrm{F}} < 0.12$, the PVSA process cannot compete with the CanSOLV process even if the ideal adsorbent can be made. Again, it is important to point out that the energy value of absorption was obtained from an experimental pilot-scale system, whereas all the values for the PVSA processes are considering the "best-possible" scenarios. If pressure drops in the lines, valves are considered, each of the PVSA curves will shift up, and the y_{F} value at which PVSA can be competitive with absorption will increase. The results of the productivity maximization problem are shown in Fig. 3 (b). Since there are no theoretical limits, akin

to the thermodynamic minimum, there is no reference to compare the productivity values. Nevertheless, it is interesting to see that the maximum productivity curve corresponding to the 4-step with LPP process (P3) and that of the FP process (P4) are close to each other at very low values of y_F but show a modest difference at higher feed compositions.

The values of the decision variables corresponding to curves E3 and P3 for a selected set of y_F are shown in Fig 4 a) and b), respectively, as a radar plot. Each line on the radar plot represents a unique set of decision variables for the different feed compositions for E3 and P3 shown in the legends. The relative position of the lines on each spoke/radii represents the magnitude/value of that decision variable. For the case of energy minimization, the P_H value remains low, compared to the range over which the optimizer could have chosen. This relates to the fact that pressurizing the feed any more than what is required to meet the US-DOE targets results in higher energy consumption. The values of P_L again are low enough. The feed velocity has converged to a value that is not close to either bound. Increasing the velocity any further results in increased pressure drop in the adsorption step resulting in additional energy consumption. With respect to the material properties, the optimizer converged on values of q_{sat} that were not close to either bound. The N_2 affinity parameter, b_{N_2}, has converged to very low values, reiterating that negligible N_2 adsorption favours lower energy consumption[15,16]. The CO_2 affinity parameter also puts the isotherms closer to in a linear region. These are also confirmed by the ΔU values that have both converged to the lower bounds. Fig 4 b) shows the spider plot for P3. Some salient differences compared to Fig 4 a) can be noticed. The P_H values converged at the upper bound, while the P_L values did not go to their minimum. The behaviour of the P_H values is rather understandable as the optimizer tends to maximize the so-called working capacity. However, the behaviour of P_L values highlights a subtle aspect that is associated with the dynamics of the vacuum pump. Since we have assumed a constant volumetric flow of the pump, it is understandable that the pump would need to run longer in order to evacuate a given amount (moles) of the product compared to operation at higher pressures. This results in longer cycle times that act to

reduce productivity. The v_F in all cases has now converged at its maximum limit in-order to increase productivity. It is also worth noting that q_{sat} values have hit the upper bound as the optimizer tries to maximize the working capacity. The corresponding ΔU values consistently converge to their lower bound. The corresponding CO_2 and isotherms are plotted, along with the isotherms of the three real adsorbents, in Fig. 4. Since the N_2 affinity in all cases was negligible, its isotherms are not shown. It can be seen that all isotherms are closer to being linear and the capacities for P3 are larger than those for E3. This clearly points to the fact that very nonlinear isotherms are not desired as they adversely affect processes that require low vacuum pressures. These observations are consistent with other studies[31].

In Case study 2, the key question posed was, "*How does the performance of real adsorbents compare to the limits determined in Case study 1?*". Three adsorbents were considered, namely, zeolite 13X (the current benchmark material), IISERP-MOF2, a MOF that was found to provide the minimum energy from an extensive search of the literature[6], UTSA-16, another well-studied MOF that has been known to provide low energy consumption. Each of these materials was fitted to a Langmuir isotherm and was used in the optimization (see Table S3 for parameters). Since the material properties are fixed, only process variables were chosen as decision variables for these optimization runs. Figure 3 (c) compares the performance of these three materials with the achievable limit (E3). Of the three, IISERP-MOF2 (E5) performs the best, followed by UTSA-16 (E6) and Zeolite 13X (E7). From the perspective of minimum energy, the difference between the two MOFs is rather marginal. This trend confirms earlier studies that have attributed the superior performance of the two MOFs to their lower N_2 affinities.[6]. The gap between E3 and E5 can be considered as the innovation gap for material development. Within the range $y_F = 0.1$ to $y_F = 0.45$, the difference between the curves E5 and E3 reduces from $\approx 20\%$ to 2.5%. This is an interesting result that shows that in the range of operating conditions at which PVSA may be favourable, i.e., at high y_F, the material innovation-gap is very small, indicating that further improvements in material development can be very challenging, and the focus will need to be on other

attributes such as stability, sensitivity to moisture, cost, etc. Figure 3 (d) shows maximum achievable productivity for the three materials. The productivity achievable using Zeolite 13X (P7) is very low compared to the others. Unlike the case of energy, where the higher N_2 affinity contributed to the higher energy consumption, in the case of productivity, the impeding factor is the higher non-linearity of the CO_2 isotherm. Vacuum pumps take a longer time to evacuate columns filled with materials that have a nonlinear isotherm and this leads to lower productivity. This is highlighted in Fig. 4 d). Further, the innovation gap in terms of productivity shows the opposite trend compared to energy. In other words, at lower values of y_F, IISERP is close to the achievable target, but at higher values of y_F, there seems to be some opportunity to innovate.

In Case study 3, the key question posed was "*How does the recovery constraint affect the achievable limits?*". The CO_2 recovery is a key constraint that can have a major impact on the performance[35]. In this case, the assumption is that all the feed enters the adsorption column, but the process operating conditions can be altered such that the target CO_2 recovery can be achieved. The typical US-DOE requirement is 90%, while for deep-decarbonization scenarios, higher recoveries are desired and if the goal is to reduce the cost of CO_2 capture, lower recoveries might be tolerated. In this case study, the recovery constraint was set at 70, 80 and 95% while maintaining $Pu_{CO_2} \geq 95\%$. The difference between the 95% case (E10) and the 90% case (E3) is much larger than the difference between the 90% (E3) and 80% (E9). This trend is consistent with previous studies which showed that the energy consumption increases exponentially with the recovery[35]. It is also interesting to note that at 95% recovery, the minimum energy limit corresponding to $y_F = 0.15$, i.e., corresponding to flue gas from coal plants is comparable to that of absorption. The productivity limits are shown in Fig. 3 (f). The trends are similar to the energy values. High productivity gains can be achieved when the recovery constraint is relaxed from 95 to 90%. Below that, the gains are modest.

In Fig. 2, we explored the pressure ranges that will satisfy US-DOE targets. In case study

4, we move a step further and ask "*How does the low pressure affect the performance?*". The achievable energy limits are shown in Fig. 3 (g). For this study, we considered three additional lower bounds for the low-pressure, namely, 0.1 bar (E11), 0.25 bar (E12) and 0.4 bar (E13). There is a significant difference between E3 and E11. This arises from the fact that in order to achieve the US-DOE targets, the flue gas has to be pressurized, and the energy consumption for that step is quite high. It is worth pointing out that if we are restricted to $P_{\mathrm{L}} \geq 0.1$ bar, the achievable energy, corresponding to $y_{\mathrm{F}} = 0.18$, exceeds the reboiler energy in absorption. This clearly indicates that PVSA is unlikely to compete with absorption processes for coal-based flue gas, even if the best adsorbent can be synthesized. For the same limit of P_{L}, the maximum achievable productivity (P11) is not markedly different compared to P3. However, constraining P_{L} to even higher values has a marked impact on productivity. The mapping of key decision variables for each case study is provided in the supporting information, along with an MS Excel file with the numerical values.

Adsorbent limits: The previous sections explored the practically achievable limits, where we solved the inverse problem. In this section, we attempt to explore the forward problem, i.e., how materials properties map to process performance, specifically using the 4-step with LPP cycle. Within the materials properties, we focus our attention on the isotherms of CO_2 and N_2. As seen earlier, the Langmuir isotherms for two components can be described using five parameters. For ease of visualization, we fix three of them. From the inverse problem solutions, we observed that the $|\Delta U|$ for both components reached its minimum limit, and accordingly, we fix them to $|\Delta U_{\mathrm{CO_2}}|$=7 kJ/mol and $|\Delta U_{\mathrm{N_2}}|$=3 kJ/mol. We also fix the q_{sat} values for both components to 6 mol/kg (comparable to those of Zeolite 13X). In this context, the isotherms of the two components can be completely specified by the Henry constants of the two components, $H_{\mathrm{CO_2}}$ and $H_{\mathrm{N_2}}$. At this point, several combinations of $H_{\mathrm{CO_2}}$ and $H_{\mathrm{N_2}}$ can be generated and each pair represents a hypothetical material, whose isotherms can be fully reconstructed using the five isotherm parameters. The plot of $H_{\mathrm{CO_2}}$ vs. $H_{\mathrm{N_2}}$ is called the nonlinearity plot (NLP) as it denotes the nonlinearity of the isotherms[15].

Since the q_{sat} value is fixed, a low value of H_i represents a linear isotherm and a high value denotes a nonlinear isotherm. Note that in the NLP, since CO_2 is considered as the stronger component, only the region above the diagonal is feasible. Further, any line parallel to the diagonal represents hypothetical materials with identical selectivities ($\alpha = H_{CO_2}/H_{N_2}$). As expected, the diagonal represents $\alpha = 1$.

Case study 5 concerns the question *"For a fixed composition, what is the practically achievable minimum energy and maximum productivity for each hypothetical material?"*. In this case study, for each material, i.e., a combination of H_{CO_2} and H_{N_2}, the process variables were treated as decision variables, and the objective functions were set to either minimize energy or maximize productivity, both subject to US-DOE targets. The results are depicted in the NLP, as shown in Fig. 5 (a) and (b) for $y_F = 0.15$. The region denoted by the grey dots was explored, but the optimizer was not able to fulfil the US-DOE constraints. Within the range of values where feasible conditions were found, many interesting observations can be made. First, materials with fixed values of α do not result in identical performance. For instance, consider materials with $\alpha = 1000$. At the bottom left, we have a region where the US-DOE targets are not met, then we pass through a region where the separation is feasible, but the energy consumption is high, then a region where energy consumption reduces, and then another region where the energy increases. Finally, we are back in a region where the US-DOE targets are not met. A very similar trend is observed when considering productivity values. This clearly indicates that the selectivity, which is often used as a parameter to screen materials, does not provide a good correlation to the process performance. Second, the behaviour described here can be rationalized by understanding that in the bottom left of the NLP, it is not possible to achieve separation because of the low CO_2 affinity and at the top right of the figure, the limitation comes from the high N_2 affinity. Hence, it is clear that, even at a fixed value of α, there is an optimal value of H_{CO_2} and H_{N_2} where the energy is minimized (or the productivity is maximized). Now, let us consider traversing along a path where H_{N_2} is fixed, say at $H_{N_2} = 10^{-4}$ m^3/kg. Close to the diagonal, there

is a region where the targets are not achieved. As we move up, i.e., as H_{CO_2} increases, we traverse through a region where the energy is first high, then decreases, and finally increases again. In other words, the energy goes through a minimum with H_{CO_2}. Similarly, when considering Fig. 5 b, the productivity goes through a maximum. At lower values of H_{CO_2}, the separation is challenging and hence very high values of energy need to be spent. Beyond the minimum, as the Henry constant increases, the isotherm becomes more nonlinear, and since the operating pressure range is fixed (as it would be in a real process), the working capacity decreases. This translates into poorer performance. Finally, let us consider points that lie on a constant H_{CO_2} value. As we move from higher values of H_{N_2} to lower values, the performance improves. This observation is consistent with previous observations that pointed to the fact improvement of the performance of materials can be achieved by aiming to reduce N_2 adsorption. Finally, it is also worth noting that within the region where the DOE targets are met, there is a wide variation in the energy consumption, i.e., between ≈ 150 to 400 kWh_e/tonne CO_2 cap. with the minimum around $\alpha = 1000$ and $H_{CO_2} \approx 0.033 m^3/kg$. Interestingly, this region also corresponds to where the maximum productivity is achieved. Hence, from both the energy and productivity perspectives, this region appears to be optimal for $y_F = 0.15$. Note that the IISERP-MOF2 and UTSA-16 are closer to this region, while Zeolite 13X is further away. Comparing their relative performances from Fig. 3, the trends seem consistent.

In case study 6, the key question was, *"How does the NLP vary when the feed composition is changed?"*. Hence, the optimization reported in Fig. 5 (a) and (b) was repeated, now for feed compositions of 0.25. The results are shown in Fig. 5 (c) and (d). All the qualitative trends observed in Fig. 5 (a) and (b) are also observed when the feed composition is increased. However, it is worth noting that the region of feasible separation is now, understandably, enlarged. Note that the energy values are much lower, and the productivity values are higher compared to the results for $y_F = 0.15$. Finally, the energy and productivity landscape seems to be much shallower compared to the case of $y_F = 0.15$. In other words, a much broader

range of H_{CO_2} and H_{N_2} values result in comparable values of energy (or productivity) than the case of $y_F = 0.15$. The corresponding values of P_H and P_L, for each hypothetical adsorbent is provided in Figs. S5 and S6 of the supporting information.

Perspective: This study shows that it will be challenging for PVSA processes to outcompete established absorption-based processes when CO_2 composition in the feed is below $y_F = 0.15$. At higher feed compositions, PVSA seems to have a clear opportunity to offer lower energy consumption compared to absorption, with the possibility of operating at practical vacuum conditions. However, in this range, the innovation gap between existing materials to the hypothetical best in terms of energy is marginal. It is worth noting that this study considers PVSA processes using beaded adsorbents that follow a Langmuir isotherm. While these can be considered as limitations, it is worth pointing out that most current work on material development can be reasonably captured within these assumptions. Hence, we argue that the results of this study can have broad implications for both adsorbent and process development. It is also important to note that the ability of an adsorbent is not just dependent on its ability to concentrate CO_2 from N_2. Other factors, including, but not limited to, stability, inertness to impurities and moisture, and structurability, play a critical role, and the optimal adsorbent is often a compromise of many parameters. Nevertheless, this work provides broad guidelines on what practical limitations exist and where future research could be focused on. While we have considered only performance metrics in this work, challenges in scaling-up the processes especially for treating large flue gas volumes should not be underestimated[21]. We have to caution the reader not to extrapolate the conclusions made here for other adsorption separation processes, e.g., TSA, since they operate on very different principles. Finally, the study reiterates the need for synergistic development of processes and materials and highlights the possibilities that could arise through the use of machine learning tools.

Acknowledgements

Funding from Canada First Excellence Research Fund through University of Alberta's Future Energy systems and through the Discovery Grants program of the Natural Sciences and Engineering Research Council of Canada (NSERC) are acknowledged. Vinay Prasad acknowledges support from the Jaffer professorship in Process Systems and Control Engineering. Computations reported in this work were supported by Compute Canada's through the resources for research groups competition.

Supporting Information

Supporting Information containing governing equations, boundary conditions, expressions to calculate performance indicators, distributions of inputs for training data, R^2_{Adj} for various performance indicators, adsorption isotherm parameters, classification results and the comparison of energy values for the adsorbents studied, excel file containing numerical values of results shown in each figure are available free of cost through the ACS Website. Training data and MATLAB code for adsorbent screening using MAPLE can be obtained by emailing the corresponding author.

Nomenclature

Roman Symbols

b, b_0	adsorption equilibrium constant [m^3 mol^{-1}]
C	fluid phase concentration [mol m^{-3}]
En	energy consumption [kWh^e tonne CO_2 cap]
H	Henry constant [-]
i	component [-]
P	pressure [bar]
Pu_{CO_2}	CO_2 product purity [%]
Pr	productivity [mol m$^-$3ads s$^-$1]
q^*	equilibrium solid phase loading [mol m^{-3}]
q_{sat}	solid phase saturation capacity [mol kg^{-1}]
R_g	universal gas constant [J mol^{-1} K^{-1}]
Re_{CO_2}	CO_2 recovery [%]
R^2	coefficient of determination [-]
t	time [s]
T	temperature [K]
ΔU	internal energy of adsorption [J mol^{-1}]
v	interstitial velocity [m s^{-1}]
y	composition in stream [-]

Abbreviations, Subscripts and Superscripts

Adj	adjusted
ADS	adsorption
ANN	artificial neural network
BLO	blowdown

CCS	carbon capture and storage
COF	covalent-organic framework
CSS	cyclic steady state
DOE	United States Department of Energy
DSL	dual-site Langmuir
EVAC	evacuation
F	feed
FP	feed pressurization
H	high pressure
I	intermediate pressure
LDF	linear driving force
L	low pressure
LPP	light product pressurization
MAPLE	machine-assisted adsorption process learning and emulation
MOF	metal-organic framework
NSGA	non-dominated sorting genetic algorithm
Opt.	optimization
PSA	pressure swing adsorption
PVSA	pressure vacuum swing adsorption
SSL	single-site Langmuir
TSA	temperature swing adsorption
VSA	vacuum swing adsorption

References

1. IPCC, Global Warming of 1.5° C. An IPCC Special Report on the Impacts of Global Warming of 1.5° C Above Pre-Industrial Levels and Related Global Greenhouse Gas Emission Pathways, in the Context of Strengthening the Global Response to the Threat of Climate Change, Sustainable Development, and Efforts to Eradicate Poverty. 2018.

2. Bui, M.; Adjiman, C. S.; Bardow, A.; Anthony, E. J.; Boston, A.; Brown, S.; Fennell, P. S.; Fuss, S.; Galindo, A.; Hackett, L. A.; Hallett, J. P.; Herzog, H. J.; Jackson, G.; Kemper, J.; Krevor, S.; Maitland, G. C.; Matuszewski, M.; Metcalfe, I. S.; Petit, C.; Puxty, G.; Reimer, J.; Reiner, D. M.; Rubin, E. S.; Scott, S. A.; Shah, N.; Smit, B.; Trusler, J. P. M.; Webley, P.; Wilcox, J.; Mac Dowell, N. Carbon capture and storage (CCS): the way forward. *Energ. Environ. Sci.* **2018**, *11*, 1062–1176.

3. Webley, P. A. Adsorption technology for CO_2 separation and capture: a perspective. *Adsorption* **2014**, *20*, 225–231.

4. Samanta, A.; Zhao, A.; Shimizu, G. K.; Sarkar, P.; Gupta, R. Post-combustion CO_2 capture using solid sorbents: A review. *Ind. Eng. Chem. Res.* **2011**, *51*, 1438–1463.

5. Rajagopalan, A. K.; Avila, A. M.; Rajendran, A. Do adsorbent screening metrics predict process performance? A process optimisation based study for post-combustion capture of CO_2. *Int. J. Greenh. Gas Con.* **2016**, *46*, 76–85.

6. Burns, T. D.; Pai, K. N.; Subraveti, S. G.; Collins, S. P.; Krykunov, M.; Rajendran, A.; Woo, T. K. Prediction of MOF Performance in Vacuum Swing Adsorption Systems for Postcombustion CO_2 Capture Based on Integrated Molecular Simulations, Process Optimizations, and Machine Learning Models. *Env. Sci. Technol.* **2020**, *54*, 4536–4544.

7. Leperi, K. T.; Chung, Y. G.; You, F.; Snurr, R. Q. Development of a general evaluation metric for rapid screening of adsorbent materials for postcombustion CO_2 capture. *ACS Sus. Chem. Engg.* **2019**, *7*, 11529–11539.

8. Farmahini, A. H.; Krishnamurthy, S.; Friedrich, D.; Brandani, S.; Sarkisov, L. From crystal to adsorption column: challenges in multiscale computational screening of materials for adsorption separation processes. *Ind. Engg. Chem. Res.* **2018**, *57*, 15491–15511.

9. Park, J.; Rubiera Landa, H. O.; Kawajiri, Y.; Realff, M. J.; Lively, R. P.; Sholl, D. S. How well do approximate models of adsorption-aased CO_2 capture processes predict results of detailed process models? *Ind. Engg. Chem. Res.* **2019**, *59*, 7097–7108.

10. Brandani, S.; Farmahini, A. H.; Friedrich, D.; Krishnamurthy, S.; Sarkisov, L. Performance-based screening of porous materials for carbon capture. *arXiv preprint arXiv:2009.12289* **2020**,

11. Subramanian Balashankar, V.; Rajendran, A. Process Optimization-Based Screening of Zeolites for Post-Combustion CO_2 Capture by Vacuum Swing Adsorption. *ACS Sus. Chem. Engg.* **2019**, *7*, 17747–17755.

12. Khurana, M.; Farooq, S. Adsorbent screening for postcombustion CO_2 capture: a method relating equilibrium isotherm characteristics to an optimum vacuum swing adsorption process performance. *Ind. Eng. Chem. Res.* **2016**, *55*, 2447–2460.

13. Yancy-Caballero, D.; Leperi, K. T.; Bucior, B. J.; Richardson, R. K.; Islamoglu, T.; Farha, O. K.; You, F.; Snurr, R. Q. Process-level modelling and optimization to evaluate metal–organic frameworks for post-combustion capture of CO_2. *Mol. Syst. Des. Eng.* **2020**, *5*, 1205–1218.

14. Maring, B. J.; Webley, P. A. A new simplified pressure/vacuum swing adsorption model for rapid adsorbent screening for CO_2 capture applications. *Int. J. Greenh. Gas Con.* **2013**, *15*, 16–31.

15. Rajagopalan, A.; Rajendran, A. The effect of nitrogen adsorption on vacuum swing adsorption based post-combustion CO_2 capture. *Int. J. Greenh. Gas Con.* **2018**, *78*, 437–447.

16. Danaci, D.; Bui, M.; Mac Dowell, N.; Petit, C. Exploring the limits of adsorption-based CO_2 capture using MOFs with PVSA–from molecular design to process economics. *Mol. Syst. Des. Engg.* **2020**, *5*, 212–231.

17. Khurana, M.; Farooq, S. Integrated Adsorbent Process Optimization for Minimum Cost of Electricity Including Carbon Capture by a VSA Process. *AIChE J.* **2019**, *65*, 184–195.

18. Pai, K. N.; Prasad, V.; Rajendran, A. Experimentally validated machine learning frameworks for accelerated prediction of cyclic steady state and optimization of pressure swing adsorption processes. *Sep. Purif. Technol.* **2020**, 116651.

19. Leperi, K. T.; Yancy-Caballero, D.; Snurr, R. Q.; You, F. 110th Anniversary: Surrogate Models Based on Artificial Neural Networks To Simulate and Optimize Pressure Swing Adsorption Cycles for CO_2 Capture. *Ind. Engg. Chem. Res.* **2019**, *58*, 18241–18252.

20. Pai, K. N.; Prasad, V.; Rajendran, A. Generalized, Adsorbent-agnostic, artificial neural network framework for rapid simulation, optimization, and adsorbent screening of adsorption processes. *Ind. Eng. Chem. Res.* **2020**, *59*, 16730–16740.

21. Subraveti, S. G.; Roussanaly, S.; Anantharaman, R.; Riboldi, L.; Rajendran, A. Techno-economic assessment of optimised vacuum swing adsorption for post-combustion CO_2 capture from steam-methane reformer flue gas. *Sep. Purif. Technol.* **2020**, 117832.

22. Krishnamurthy, S.; Rao, V. R.; Guntuka, S.; Sharratt, P.; Haghpanah, R.; Rajendran, A.; Amanullah, M.; Karimi, I. A.; Farooq, S. CO_2 capture from dry flue gas by vacuum swing adsorption: A pilot plant study. *AIChE J.* **2014**, *60*, 1830–1842.

23. Haghpanah, R.; Nilam, R.; Rajendran, A.; Farooq, S.; Karimi, I. A. Cycle synthesis and optimization of a VSA process for postcombustion CO_2 capture. *AIChE J.* **2013**, *59*, 4735–4748.

24. Perez, L. E.; Sarkar, P.; Rajendran, A. Experimental validation of multi-objective optimization techniques for design of vacuum swing adsorption processes. *Sep. Purif. Technol.* **2019**, *224*, 553–563.

25. Ritter, J. A.; Bumiller, K. C.; Tynan, K. J.; Ebner, A. D. On the use of the dual process Langmuir model for binary gas mixture components that exhibit single process or linear isotherms. *Adsorption* **2019**, *25*, 1511–1523.

26. Lin, L.-C.; Berger, A. H.; Martin, R. L.; Kim, J.; Swisher, J. A.; Jariwala, K.; Rycroft, C. H.; Bhown, A. S.; Deem, M. W.; Haranczyk, M., et al. In silico screening of carbon-capture materials. *Nat. Mater.* **2012**, *11*, 633.

27. Farmahini, A. H.; Friedrich, D.; Brandani, S.; Sarkisov, L. Exploring new sources of efficiency in process-driven materials screening for post-combustion carbon capture. *Ener. Envi. Sci.* **2020**, *13*, 1018–1037.

28. Deb, K.; Pratap, A.; Agarwal, S.; Meyarivan, T. A fast and elitist multiobjective genetic algorithm: NSGA-II. *IEEE Trans. Evol. Comput.* **2002**, *6*, 182–197.

29. Pai, K.; Baboolal, J.; Sharp, D.; Rajendran, A. Evaluation of diamine-appended metal-organic frameworks for post-combustion CO_2 capture by vacuum swing adsorption. *Sep. Purif. Technol.* **2019**, *211*, 540–550.

30. Nikolaidis, G. N.; Kikkinides, E. S.; Georgiadis, M. C. An integrated two-stage P/VSA process for postcombustion CO_2 capture using combinations of adsorbents Zeolite 13X and Mg-MOF-74. *Ind. Eng. Chem. Res.* **2017**, *56*, 974–988.

31. Khurana, M.; Farooq, S. Integrated adsorbent-process optimization for carbon capture and concentration using vacuum swing adsorption cycles. *AIChE J.* **2017**, *63*, 2987–2995.

32. Husebye, J.; Brunsvold, A. L.; Roussanaly, S.; Zhang, X. Techno Economic Evaluation of Amine based CO2 Capture: Impact of CO_2 Concentration and Steam Supply. *En-*

ergy Procedia **2012**, *23*, 381 – 390, The 6th Trondheim Conference on CO_2 Capture, Transport and Storage.

33. Brandani, S. Carbon dioxide capture from air: a simple analysis. *Energy & Environ.* **2012**, *23*, 319–328.

34. Singh, A.; Stéphenne, K. Shell Cansolv CO_2 capture technology: achievement from first commercial plant. *Energy Procedia* **2014**, *63*, 1678–1685.

35. Maruyama, R. T.; Pai, K. N.; Subraveti, S. G.; Rajendran, A. Improving the performance of vacuum swing adsorption based CO_2 capture under reduced recovery requirements. *Int. J. Greenh. Gas Control.* **2020**, *93*, 102902.

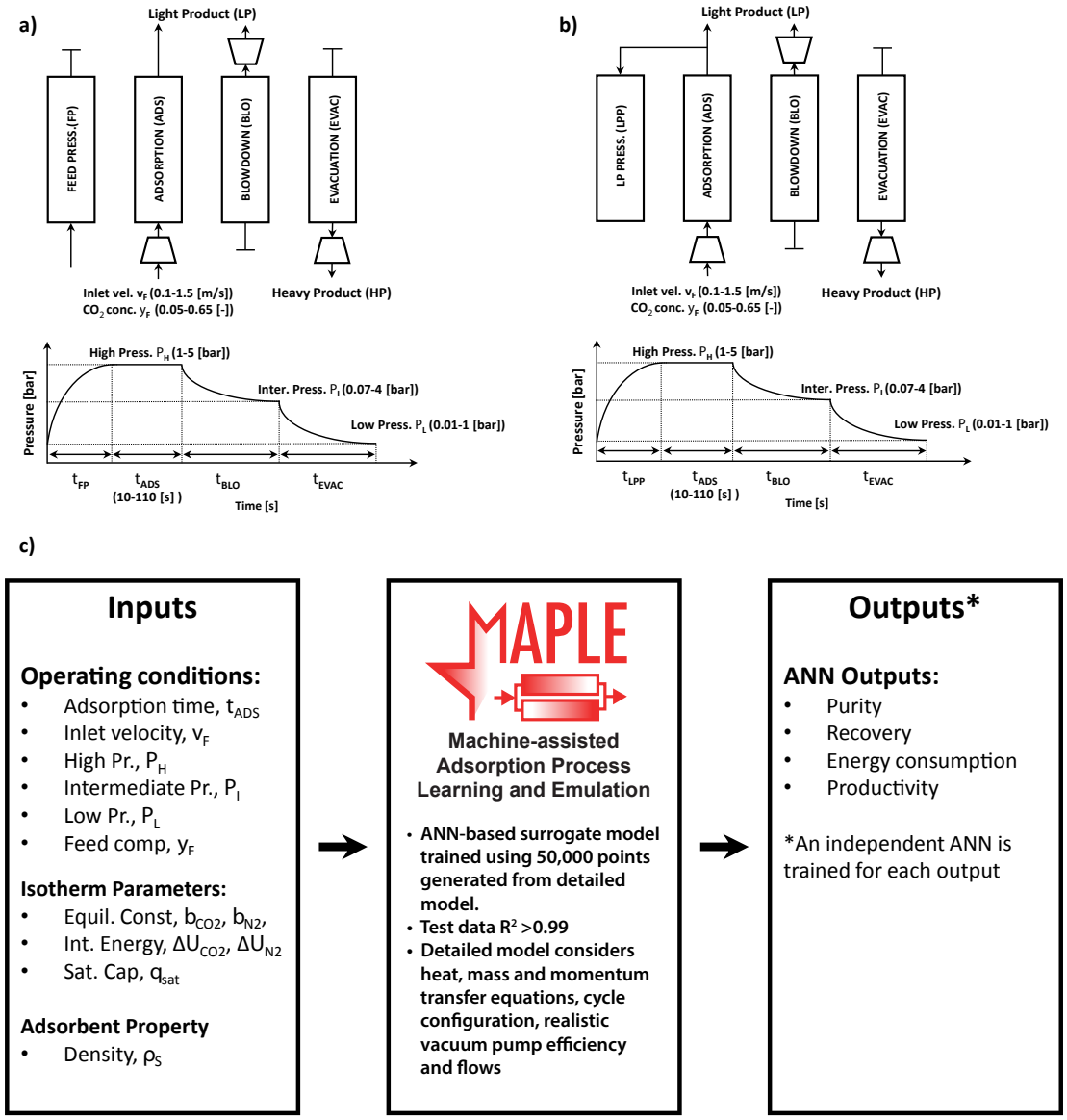

Figure 1: Process cycles used in this study a) 4-step with feed pressurization (FP), b) 4-step with light-product pressurization (LPP). c) The key components of the MAPLE framework.

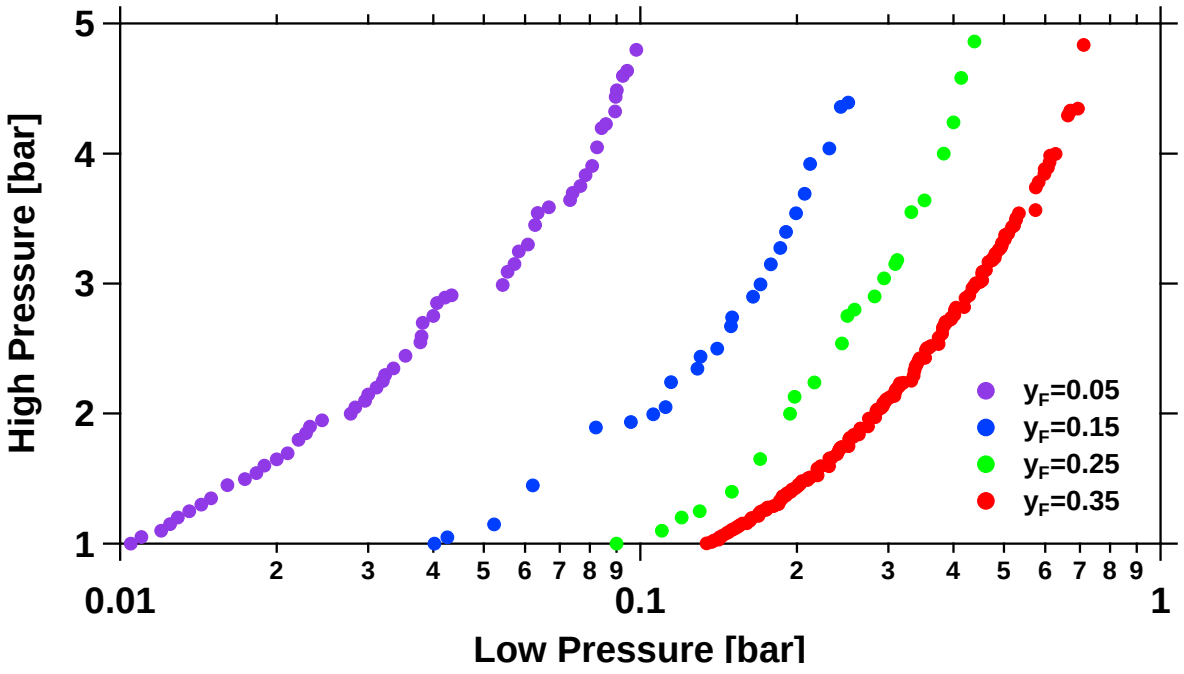

Figure 2: Pareto curves obtained from a multi-objective optimization for maximizing low-pressure (P_{L}) and minimizing high-pressure (P_{H}) to achieve US-DOE targets (CO_2 purity $> 95\%$ and recovery $\geq 90\%$)for various feed compositions using the 4-step with LPP cycle. Both operating and isotherm parameters were used as decision variables. The region to the right of each curve is infeasible.

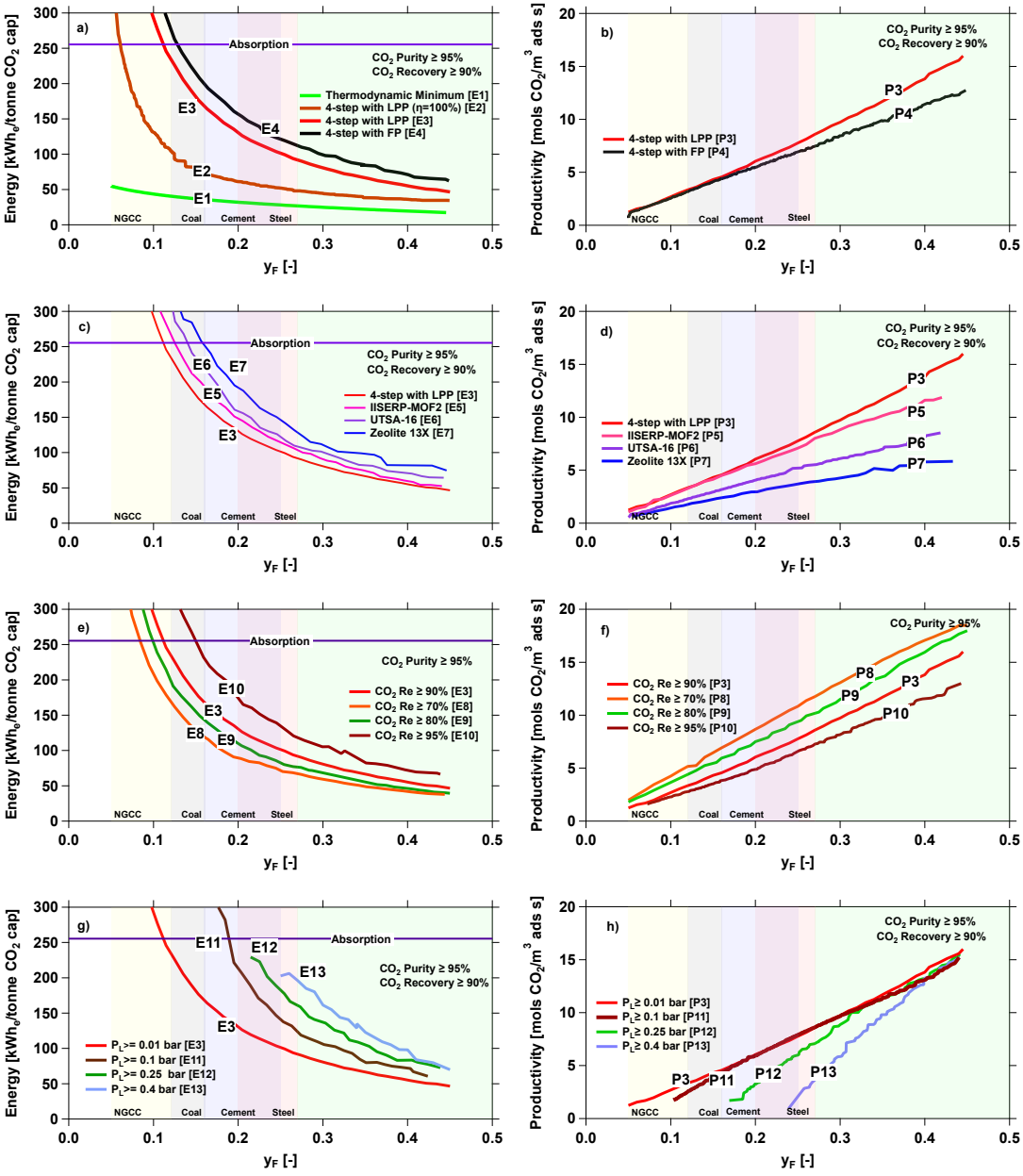

Figure 3: Practically achievable performance limits for a variety of case studies. The figures in the left column refer to minimum energy, while those on the right indicate maximum productivity case studies. a) and b) are results from case study 1, where both isotherm and process operating parameters are used as decision variables. c) and d) are results from case study 2, where the aim was to evaluate the performance of some real adsorbents with the 4-step LPP process. Here only operating parameters are used as decision variables. e) and f) are results from case study 3 that explored the impact of CO_2 recovery on the achievable limits with the 4-step LPP process. Here both isotherm and operating parameters were treated as decision variables. g) and h) are results from case study 4 that explored the impact of the low pressure with the 4-step LPP process. Here both isotherm and operating parameters were treated as decision variables. The reboiler duty for adsorption was obtained from the literature[34] and a 40% efficiency was used to convert from thermal to electrical units. Note: 100 kWh/tonne= 0.36 GJ/tonne, 10 $\mathrm{mol_{CO_2}/m^3}$ ads s 38 $\mathrm{tonne_{CO_2}/m^3}$ ads day

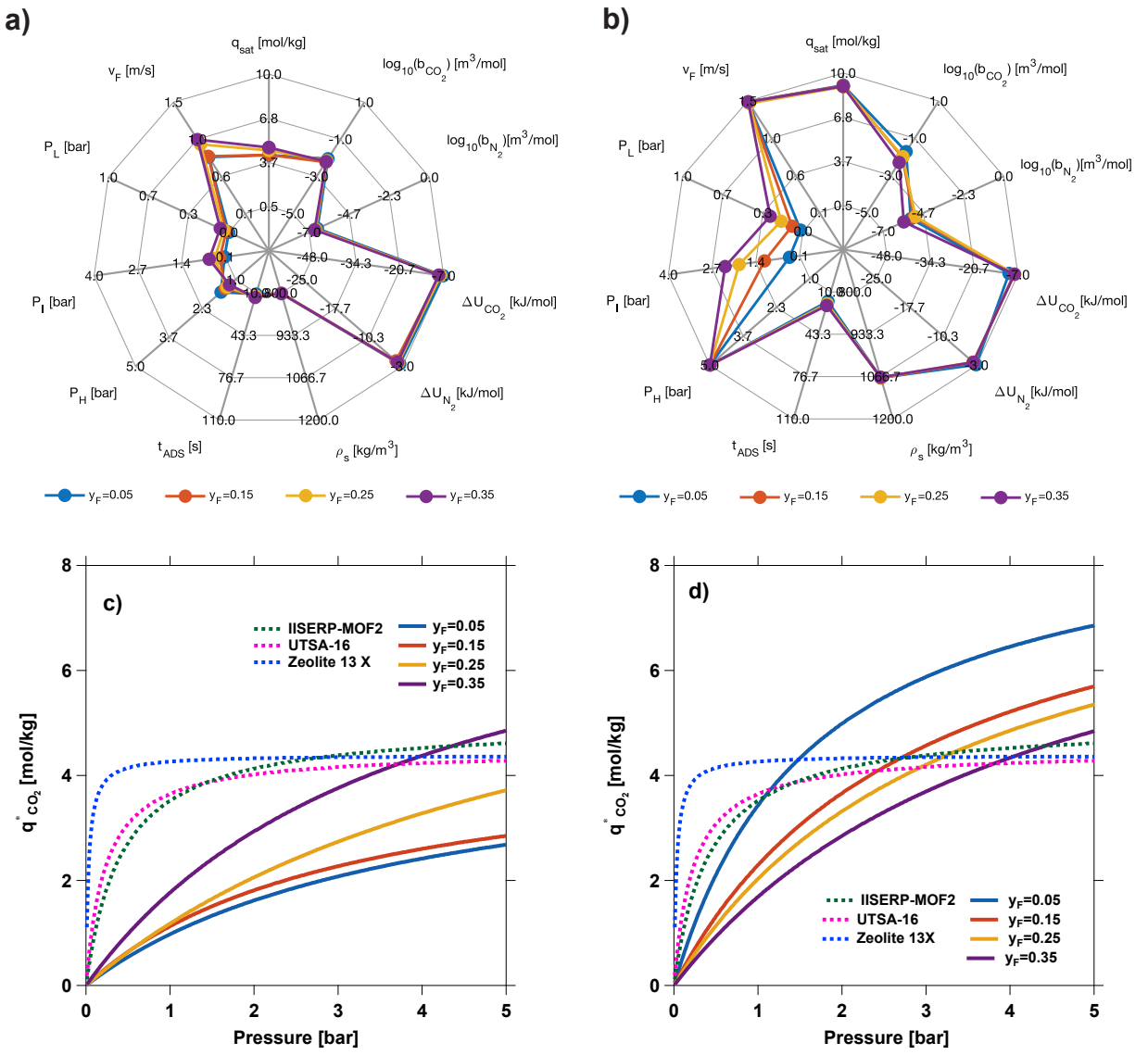

Figure 4: Mapping of decision variables corresponding to curves E3 and P3in Fig. 3. a) Radar plot of decision variables corresponding to minimum energy (i.e., curve E3 in Fig 3), and b) Radar plot of decision variables corresponding to maximum productivity (i.e., curve P3 in Fig 3). c) and d) show the isotherms of CO_2 (and N_2, its very low) corresponding to isotherm parameters shown in a) and b). The plot of the isotherms shown in a) and b) along with those of the three real adsorbents studied are shown in sub-figures c) and d), respectively.

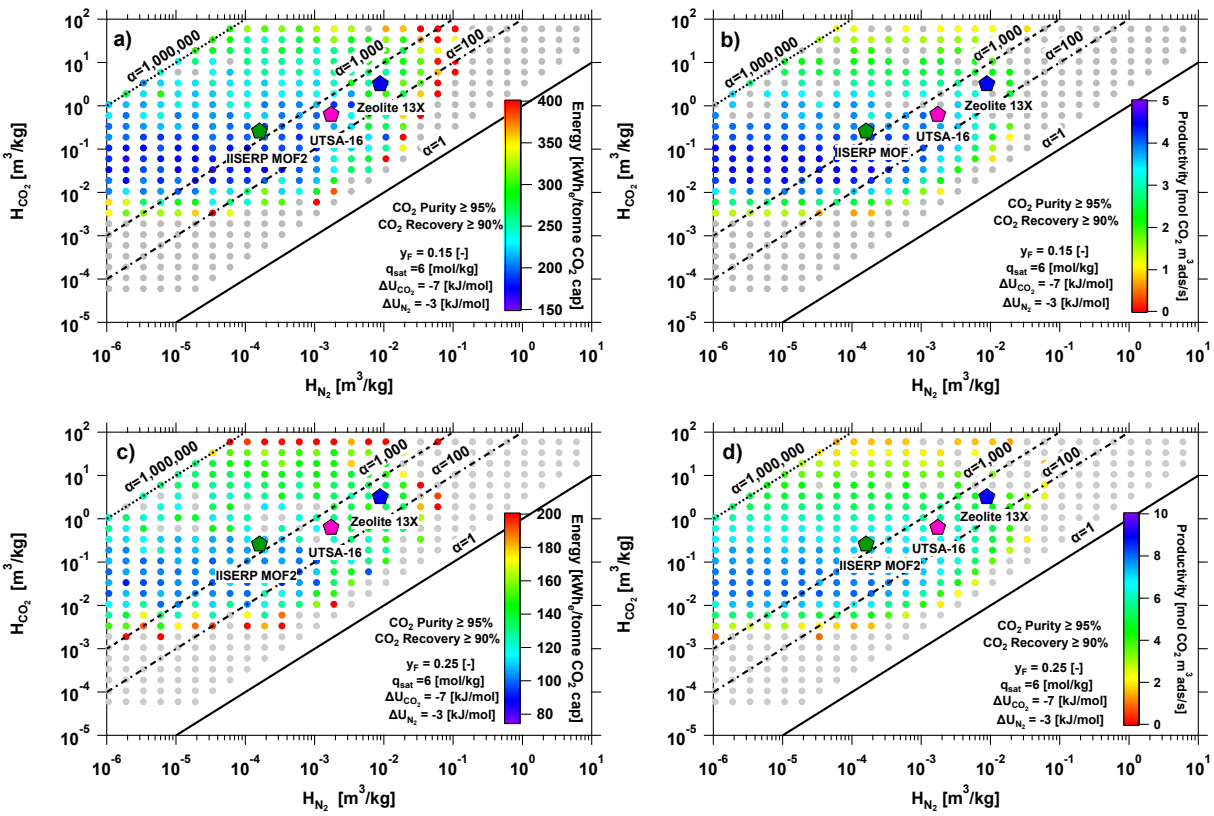

Figure 5: The impact of adsorption isotherm on process performance. The subplots a) and c) show minimized energy, while b) and d) show maximized productivity of the 4-step with LPP cycle. For each combination of $H_{\mathrm{CO_2}}$ and $H_{\mathrm{N_2}}$, the process operating conditions are optimized to either minimize energy or maximize productivity. The diagonal lines on the plot represent the lines of constant selectivity, the symbols correspond to the adsorbents used in this study as a reference. Note that the isotherm parameters for these materials are provided in the supporting information. The results are shown for two different feed compositions $y_{\mathrm{F}} = 0.15$ (top row), $y_{\mathrm{F}} = 0.25$ (bottom row)

Table 1: Parameters used for detailed model simulations. Those indicated as variable are used for training the MAPLE framework and used as decision variables.

Parameter	**Type**	**Value**
Column properties		
Bed length, L [m]	Fixed	1.0
Column inner radius, r_{in} [m]	Fixed	0.14
Column outer radius, r_{out} [m]	Fixed	0.16
Particle voidage, ϵ_{p} [-]	Fixed	0.35
Particle radius, r_{p} [m]	Fixed	1×10^{-3}
Density of the column wall, ρ_{w} [kg m^{-3}]	Fixed	7,800.00
Bed voidage, ϵ [-]	Fixed	0.37
Tortuosity factor, τ [-]	Fixed	3.00
Fluid properties		
Effective heat conduction coefficient, K_{z} [J m^{-1} s^{-1} K^{-1}]	Fixed	9.03 $\times10^{-2}$
Thermal conductivity of the wall, K_{w} [W m^{-1} K^{-1}]	Fixed	16.00
Inside heat transfer coefficient, h_{in} [W m^{-2} K^{-1}]	Fixed	0.00
Outside heat transfer coefficient, h_{out} [W m^{-2} K^{-1}]	Fixed	0.00
Gas specific heat capacity, $C_{\text{p,g}}$[J kg^{-1} K^{-1}]	Fixed	1010.60
Adsorbed phase specific heat capacity, $\text{C}_{\text{p,a}}$ [J kg^{-1} K^{-1}]	Fixed	1010.60
Adiabatic constant, γ [-]	Fixed	1.40
Universal gas constant, R_g [m^3 Pa mol^{-1} K^{-1}]	Fixed	8.314
Fluid viscosity, μ [kg m^{-1} s^{-1}]	Fixed	1.72×10^{-5}
Molecular diffusivity, D_{M} [m^2 s^{-1}]	Fixed	1.60×10^{-5}
Adsorbent properties		
Adsorbent specific heat capacity, $C_{\text{p,s}}$ [J kg^{-1} K^{-1}]	Fixed	1070.00
Density of the solid particle, ρ_{s} [kg m^{-3}]	Variable	800.00-1200.00
Adsorption saturation capacity, q_{sat} [mol kg^{-1}]	Variable	0.50 to 10.00
Adsorption equilibrium constant of CO_2, b_{0,CO_2} [m^3 mol^{-1}]	Variable	10^{-12} to 10^{-1}
Adsorption equilibrium constant of N_2, b_{0,N_2} [m^3 mol^{-1}]	Variable	10^{-11} to 10^{-1}
Internal energy of adsorption of CO_2, ΔU_{CO_2} [kJ mol^{-1}]	Variable	-7.00 to -47.00
Internal energy of adsorption of N_2, ΔU_{N_2} [kJ mol^{-1}]	Variable	-3.00 to -25.00
Process properties		
Feed temperature, T_{F} [K]	Fixed	298.15
Blowdown step vacuum pump flow-rate, v_{BLO} [m s^{-1}]	Fixed	0.59
Evacuation step vacuum pump flow-rate, v_{EVAC} [m s^{-1}]	Fixed	0.90
Pressurization step exponential pressure history term, α_{PRESS} [s]	Fixed	0.50
Vacuum pump efficiency, η [%]	Variable	$\frac{15.84P}{1+19.8P}$
Adsorption step time, t_{ADS} [s]	Variable	10.00 to 110.00
High pressure, P_{H} [bar]	Variable	1.00 to 5.00
Intermediate pressure, P_{I} [bar]	Variable	0.07 to 4.00
Evacuation pressure, P_{L} [bar]	Variable	0.01 to 1.00
Feed rate, v_{F} [m s^{-1}]	Variable	0.10 to 1.50
CO_2 feed composition, y_{F} [-]	Variable	0.05 to 0.65

Table 2: The data from the fitting of the various optimizations cases discussed in Fig. 3 to performance indicator (PI), PI = $\alpha e^{\beta y_F}$. Energy values are in (kWh_e/tonne CO_2 cap) and productivity values are in (mol_{CO_2}/m^3 ads s). These fits are valid for values of y_F between 0.05 and 0.45. However for the cases of E11, E12, E13, P11, P12, P13, the applicable ranges are provided in Fig. 3

Curve #	**Constraints** $[Pu_{CO_2}/Re_{CO_2}]$	α	β
E1	95/90	14.590	-0.458
E2	95/90	11.669	-1.078
E3	95/90	19.594	-1.182
E4	95/90	21.723	-1.186
E5	95/90	20.301	-1.235
E6	95/90	23.645	-1.119
E7	95/90	25.097	-1.262
E8	95/70	14.286	-1.170
E9	95/80	15.013	-1.230
E10	95/95	22.046	-1.297
E11	95/90	16.725	-1.554
E12	95/90	19.096	-1.616
E13	95/90	15.896	-1.923
P3	95/90	40.185	1.159
P4	95/90	32.633	1.115
P5	95/90	33.760	1.136
P6	95/90	21.734	1.257
P7	95/90	15.388	1.040
P8	95/70	43.780	1.014
P9	95/80	42.668	1.089
P10	95/95	33.558	1.186
P11	95/90	47.347	1.335
P12	95/90	72.070	1.799
P13	95/90	152.800	2.694

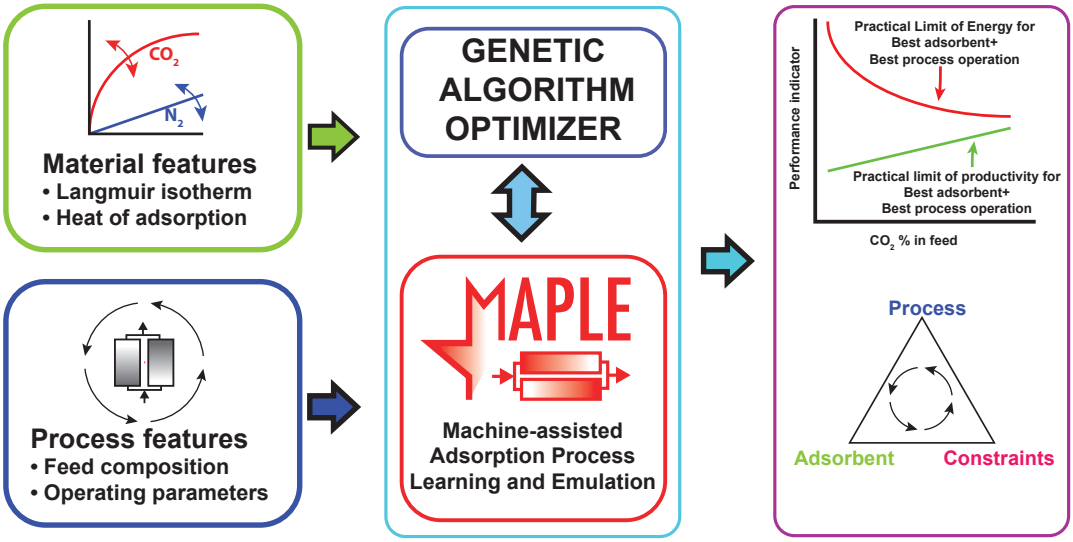

Table of Contents Figure